https://doi.org/10.5194/essd-2026-136
Preprint. Discussion started: 4 March 2026

Open Access Earth System Science Data Discussions

A random forest isoscape model of bioavailable Sr for South America: a focus on southern Brazil

Cinzia Scaggion[1], Tommaso Giovanardi[1*], László Palcsu[2], Daniel Loponte[3], Mirian Carbonera[4], Sara Bernardini[5,1], Stefano Benazzi[5], Giulia Marciani[5], Marcos Cesar Pereira Santos[6], Eugenio Bortolini[5], Anna Cipriani[1,7], Federico Lugli[1,8]

[1] Department of Chemical and Geological Sciences, University of Modena and Reggio Emilia, via Campi 103, I-41125 Modena, Italy.

[2] ICER Centre, HUN-REN Institute for Nuclear Research, Bem square, 18/C 4026 Debrecen, Hungary

[3] Consejo Nacional de Investigaciones Científicas y Técnicas (CONICET), Instituto Nacional de Antropología y Pensamiento Latinoamericano (INAPL), 3 de Febrero 1370/78 Buenos Aires, Argentina.

[4] Programa de Pós-graduação em Ciências Ambientais e Centro de Memória do Oeste de Santa Catarina da Universidade Comunitária da Região de Chapecó (Unochapecó), Rua Senador Atílio Fontana, 591 E Efapi, 89809000 - Chapecó, SC Brazil.

[5] Department of Cultural Heritage, University of Bologna, via degli Ariani 1, I-48121 Ravenna, Italy.

[6] Instituto de Ciências da Sociedade, Curso de Arqueologia, Universidade Federal do Oeste do Pará, Santarém, Brazil.

[7] Lamont-Doherty Earth Observatory of Columbia University, Palisades, New York, United States of America.

[8] Institut für Geowissenschaften, Goethe-Universität Frankfurt, Frankfurt am Main, Germany.

*corresponding author

E-mail: tommaso.giovanardi@unimore.it (TG)

Abstract

In recent years, advances in machine learning have greatly improved the generation of maps showing the geographic distribution of isotope ratios (isoscapes), which have become essential tools for environmental, mobility and provenance studies in both modern and archaeological contexts. Among the various isotopic systems employed, strontium (Sr) is particularly useful because its $^{87}Sr/^{86}Sr$ ratio in the environment is largely controlled by the underlying geology through the composition of local soils and rocks.

https://doi.org/10.5194/essd-2026-136
Preprint. Discussion started: 4 March 2026

Open Access Earth System Science Data Discussions

In this work, we present a new dataset of bioavailable $^{87}Sr/^{86}Sr$ ratios derived from n = 233 plant samples collected across southern Brazil, covering the states of Santa Catarina and Rio Grande do Sul (c.a. 370,000 km^2). The measured ratios span from 0.70521 to 0.76039 and capture the bioavailable Sr isotope signatures over all major geological units in the region.

We combined these new data with an extensive compilation of published bioavailable Sr measurements from across South America (including plants, fauna, ancient human remains, shells, snails, lichens, water and soils) to construct three random forest Sr isoscapes using different subsets of the combined dataset at the regional and continental scales. The first model incorporates the entire dataset ('All' dataset, n = 883 sites), the second is based on plant+fauna+lichen+human (n = 661 sites) and the third is limited to plant+lichen samples (n = 531 sites). Among the three models, the full dataset model shows lower predictive power, while the plant+fauna+lichen+human and the plant+lichen models yield better results, with similar RMSE (0.0049 and 0.0054) and R^2 values (ca. 0.76). Compared to existing Sr isoscapes of South America, our models significantly enhance both spatial coverage and resolution of bioavailable Sr predictions, particularly in southern Brazil.

The new bioavailable Sr isotope dataset from Santa Catarina and Rio Grande do Sul states is available at https://doi.org/10.5281/zenodo.17988601 (Scaggion et al., 2025a) and the compiled literature dataset is reported as supplementary material.

1 Introduction

Maps of isotopic variability through the landscape are powerful tools used for answering questions related to migration, trade, diet, provenance, forensic investigations, and environmental changes in both modern and ancient contexts (e.g. Hobson, 1999; Benson et al., 2006; Makarewicz and Sealy, 2015; Bataille et al., 2018, 2020; Hoogerwerff et al., 2019; Lugli et al., 2022; Gigante et al., 2023; Armaroli et al., 2024, Asrat et al., 2025; Dosseto et al., 2025; Scaggion et al., 2025b).

Among the various isotopic systems, strontium (Sr) isotopes play a central role in geotracing and provenance studies of biological materials because biota obtains Sr primarily from soils derived through weathering and disaggregation of local rocks. As a result, the so-called bioavailable $^{87}Sr/^{86}Sr$ act as a proxy for the underlying geology of a region.

Radiogenic ^{87}Sr originates by β-decay of rubidium-87 (^{87}Rb), while ^{86}Sr is stable. Consequently, the $^{87}Sr/^{86}Sr$ ratio in rocks and minerals changes depending on their ^{87}Rb content, their ages and geological history providing characteristic isotopic signatures for different geological domains (Faure and Mensing, 2005; Dickin, 2018). Through alteration and pedogenetic processes, Sr ions are leached from rocks into soils and waters, where they mix with other Sr pools derived from rainfall, snow, groundwater, atmospheric deposition or anthropic activities (Vitousek et al., 1999; Voerkelius et al.,

https://doi.org/10.5194/essd-2026-136
Preprint. Discussion started: 4 March 2026

2010). These processes can shift the local Sr isotopic signature away from the original bedrock. From soil and water, Sr enters the local ecosystem (Bullen et al., 1996; Capo et al., 1998). This bioavailable Sr is passively absorbed by plant roots and transported to leaves, where Sr^{2+} substitutes for $calcium^{2+}$ (Ca) in metabolic processes (Poszwa, 2000; White and Broadley, 2003). From plants and water, the bioavailable Sr enters the local trophic chain. In vertebrates, Sr replaces Ca in the crystalline structure of carbonated-hydroxyapatite (Pors Nielsen, 2004; Bentley, 2006), the main inorganic constituent of bones and teeth (Weiner and Wagner, 1998; Hughes and Rakovan, 2002). Thus, the $^{87}Sr/^{86}Sr$ ratios of bone and dental tissues reflect those of water, plants and animals consumed, which, in turn, mirror the bioavailable isotopic signature of the environment (Schwarcz et al., 2010; Crowley et al., 2017). Although isotopic fractionation can occur along the trophic chain and through metabolic processes, its enrichment is generally minimal (Lahtinen et al., 2020) and can be effectively corrected using standard normalization protocols during mass spectrometry analysis (Fietzke and Eisenhaure, 2006; Frei and Frei, 2011; Spies et al., 2025). For this reason, the isotopic composition of low-mobility fauna and plants represents a valuable, though not exclusive, *proxy* for estimating the local bioavailable Sr isotope signatures (Spies et al., 2025). However, deciphering environmental heterogeneity and trophic complexity is not always straightforward; therefore, integrating multiple isotopic and environmental datasets is crucial for constructing robust isoscapes.

Over the last decade, advances in spatial modelling and machine learning techniques such as kriging and random forest algorithms (e.g. Bataille et al., 2018, 2020; Hoogerwerff et al., 2019; Gigante et al., 2023; Armaroli et al., 2024; Scaggion et al., 2025b; Spies et al., 2025), have significantly increased the predictive potential of isoscapes models, by linking spatial isotopic variability to environmental predictors (Bataille et al., 2020). One of the main challenges, however, remains the acquisition of spatially representative and geologically diverse samples, making well designed sampling strategies crucial for developing accurate predictive models.

Brazil represents a particularly interesting case study for Sr isoscape research, due to its geological diversity and rich archaeological and ecological history. In southern Brazil, the states of the Santa Catarina (SC) and Rio Grande do Sul (RGS) encompass various geological formations, from ancient Precambrian crystalline rocks to younger sedimentary basins, which provide a good opportunity to test the spatial resolution, robustness, and applicability of Sr isoscapes. Despite the relevance of Brazil for provenance studies in archaeology, ecology, and food authentication, to date a comprehensive isoscape of bioavailable Sr has not been produced.

In this study, we present a newly generated dataset of n = 233 plant samples, collected across SC and RGS, representing all major geological units of the region (c.a. 370,000 km^2). This dataset was integrated with a literature-based compilation of bioavailable Sr data from across South America to

https://doi.org/10.5194/essd-2026-136
Preprint. Discussion started: 4 March 2026

developed new isoscapes of bioavailable strontium ($^{87}Sr/^{86}Sr$) for South America and southern Brazil, with a focus on SC and RGS. Using a random forest machine learning model following Bataille et al. (2020), we incorporated global environmental variables described in Bataille et al. (2018, 2020) and Reich et al. (2024) to estimate spatial patterns of bioavailable $^{87}Sr/^{86}Sr$ ratios.

The sampled region represents a pivotal area for understanding the expansion of pre-Columbian populations, constituting pass-through areas that facilitated the spread of natives such as the Guaraní, who from approximately the 5th c. AD gradually occupied the continent from the Amazon to the Paraná Delta (Loponte et al., 2024) as well as the movements of Southern Brazilian Highland populations toward the coast. The geological heterogeneity of these states provides a unique natural context for investigating large-scale dynamics of mobility, settlement, and cultural interaction.

2 Geology

We focused our sampling on the southern portion of Brazil, targeting the main geological units in detail to increase the reliability and spatial resolution of the resulting Sr database and isoscape.

The study area, comprising the states of RGS and SC, represents a key segment of the South American continent. The region preserves a long and complex geological evolution, spanning from the Archean to the Cenozoic, encompassing processes of crustal growth, continental collision, sedimentary basin development, and large igneous province magmatism. A simplified overview of this geological complexity is provided in Fig. 1, modified from the 1:5000000 geological map of Brazil (Medeiros et al. 2025) downloaded from the Serviço Geológico do Brasil (https://geosgb.sgb.gov.br/geosgb/downloads.html) for use in QGis software.

https://doi.org/10.5194/essd-2026-136
Preprint. Discussion started: 4 March 2026

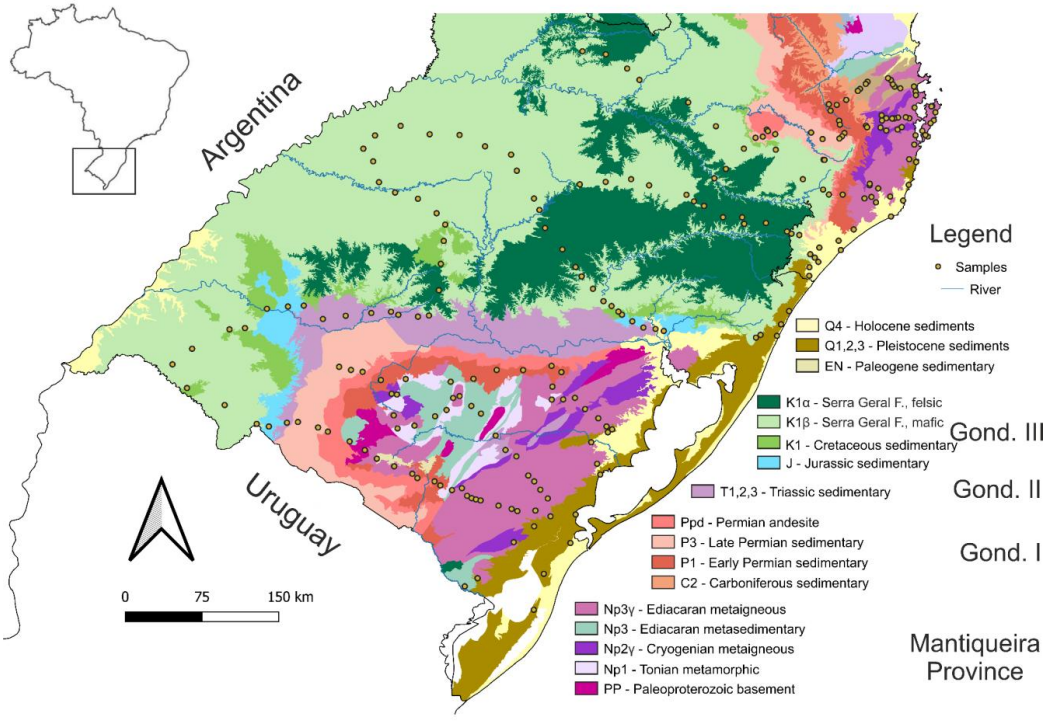

Figure 1: simplified geological map of southern Brazil, modified from Medeiros et al. (2025) with sample locations collected in this study. The lithology codes are simplified from Medeiros et al. (2025) and divided for the two main geological domains of the area: the Mantiqueira Province and the Paraná Basin. The supergroups of the latter are divided according to Milani et al. (2007).

Two major geological provinces dominate this area: the southern Brazilian Shield, representing the Precambrian crystalline basement, and the Paraná Basin, a large Paleozoic–Mesozoic sedimentary and volcanic basin. In addition to these two major geological provinces, Pleistocene and Holocene sediments outcrop along the coast and the southern lagoons of RGS.

The southern Brazilian Shield, also known as the Mantiqueira Province (Heilbron et al., 2004) is composed of a mosaic of cratonic nuclei, accreted terranes, and mobile belts that were amalgamated during the Neoproterozoic, culminating with the Gondwana accretion (Brito Neves et al., 2014). In the state of RGS, the principal tectonic domains of the Mantiqueira Province are the Dom Feliciano Belt and the São Gabriel Terrane (Brito Neves et al., 2014; Philipp et al., 2018). The Dom Feliciano Belt extends in a NE–SW orientation and consists of high-grade metamorphic complexes, syn- to post-tectonic granitic intrusions (650-540 Ma), and metavolcanic–sedimentary sequences (2.35-0.78 Ga). It is interpreted as a Neoproterozoic collisional orogen, developed during the closure of oceanic domains between the Rio de la Plata Craton and the Kalahari–Congo Craton (Brito Neves et al., 2014;

https://doi.org/10.5194/essd-2026-136
Preprint. Discussion started: 4 March 2026

Philipp et al., 2018). The belt includes the voluminous granites of the Pelotas Batholith dated between 650 and 580 Ma. The São Gabriel Terrane, located west of the Dom Feliciano Belt, comprises volcanic-arc sequences, ophiolitic remnants, and accretionary complexes. Geochemical data indicate that it represents an intra-oceanic arc formed between 900 and 700 Ma, subsequently accreted to the continental margin during the Brasiliano Orogeny (Cerva-Alvez et al., 2021). The Dom Feliciano Belt is also exposed along the coast in the eastern part of SC where it includes the Florianópolis granitic batholiths and the metavolcanic–sedimentary sequences (Brito Neves et al., 2014; Philipp et al., 2018).

The Paraná Basin is one of the world's largest intracratonic sedimentary basins, covering approximately 1.4 million km² across Brazil, Paraguay, Uruguay, and Argentina (Holz et al., 2010; Scherer et al., 2023). It developed over the consolidated Precambrian basement during a long-lived post-orogenic to extensional tectonic regime that lasted from the Ordovician to the Cretaceous.

Milani et al. (2007) divided the Paraná Basin succession into six different second-order supersequences (from oldest to youngest): Rio Ivaí, Paraná, Gondwana I, Gondwana II, Gondwana III (which includes the Serra Geral) and Bauru. In the studied area, the exposed units comprise: (1) Carboniferous-Permian volcanic-sedimentary units of the Gondwana I Supersequence (Itararé group and the Rio Bonito, Palermo and Irati formations); (2) Triassic sedimentary rocks of the Santa Maria Formation belonging to the Gondwana II Supersequence; and (3) Jurassic volcanic rocks of the Serra Geral Formation and aeolian sandstones of the Botucatu Formation, representing the Gondwana III Supersequence.

The volcanic-sedimentary units outcrop along the eastern margin of the basin, in contact with the rocks of Dom Feliciano Belt, while the volcanic rocks of Serra Geral Formation outcrop in the western part of the studied area (Fig. 1). The stratigraphic record documents alternating marine, glacial, and continental depositional environments. The major stratigraphic units include: the Itararé Group (Late Carboniferous–Early Permian) composed of glaciogenic diamictites, sandstones, and shales deposited during the Gondwanan glaciation (Holz et al., 2010); the Rio Bonito and Palermo formations (Permian) composed of coal-bearing strata deposited in deltaic and coastal-plain environments, marking post-glacial transgression (Holz et al., 2010); the Irati Formation (Late Permian) composed of organic-rich black shales and carbonates deposited under restricted marine conditions and considered one of the principal source rocks for hydrocarbons in the basin (Holz et al., 2010); the Santa Maria Formation (Triassic) composed of fluvial and aeolian sandstones (Scherer et al., 2023); and the Botucatu Formation (Jurassic) composed of cross-bedded aeolian sandstones indicative of an extensive desert environment prior to the onset of volcanism (Scherer at al., 2023).

https://doi.org/10.5194/essd-2026-136
Preprint. Discussion started: 4 March 2026

One of the main geological domains in southern Brazil is the Serra Geral Formation which records the bimodal volcanism of the Paraná-Etendeka Large Igneous Province (LIP). This volcanic province covers an area of approximately 1,200,000 km^2 in South America, extending across Brazil, Argentina, Uruguay and Paraguay, and constitutes the upper volcanic portion of the Paraná Basin (e.g. Peccerillo and Melfi, 1988). The magmatism has a bimodal character, with tholeiitic basalts and andesites as the dominant lithologies coupled with subordinate more silicic rocks (rhyodacite and rhyolite, also occurring as high-grade ignimbrites; Peate et al., 1992; Luchetti et al., 2018). The eruptive history is short, with ages constrained between 135.0 ± 0.6 Ma and 132.0 ± 0.2 Ma, with a time span of 1.6-3.0 Ma for the extrusive activity (Gomes and Vasconcelos, 2021). The Sr isotopic composition of this magmatism is extremely variable (e.g. $^{87}Sr/^{86}Sr_{130}$ between 0.705-0.728; Peate et al., 1992), reflecting significant crustal contamination during magmas ascent and/or derivation from metasomatized mantle sources (e.g. Giovanardi et al., 2022). These volcanic rocks form a plateau in the western part of the studied area separated from other geological domains by a stiff cliff.

3 Material and Methods

3.1 Materials

A total of n = 233 samples of plant leaves were collected across the study area (Fig. 1), covering all of the geological units identified on state geological maps (downloaded from the Serviço Geológico do Brasil website https://geosgb.sgb.gov.br/geosgb/downloads_en.html; geological map of Santa Catarina from Wildner et al., 2014; Rio Grande do Sul map from Wildner et al., 2013).

Sampling was designed to minimize potential contamination from agriculture, waste disposal or other anthropogenic sources. To this end, leaves were taken from trees as far as possible from anthropic activities (Spies et al., 2025). The sampled taxa include: *Eucalyptus* sp., *Phytolacca dioica*, *Neltume nigra*, *Smilax campestris*, *Celtis australis*, *Fraxinus excelsior* (Common ash) and *Nerium oleander*. Different plant taxa were intentionally collected at each location to account for different rooting depths at each location.

3.2 Isotopic analyses

Chromatographic separation of Sr was conducted at the MeGic lab (https://www.geochem.unimore.it/) of the Department of Chemical and Geological Sciences (Unimore, Italy). Leaf samples were cleaned to remove major impurities using ultrapure MilliQ® water and then dried for 24 h on a hotplate at 50°C. Approximately 20 g of dried clean plant material was reduced to ash in a porcelain crucible in a muffle oven at 650 °C for 6 h. Five milligrams of ash were then dissolved in 0.5 ml of 3M HNO_3 and centrifuged prior to loading into the chromatographic

https://doi.org/10.5194/essd-2026-136
Preprint. Discussion started: 4 March 2026

column. Sr separation was performed using a standard procedure in ~30 µl columns filled with the 100-150 µm bead size Eichrom Sr-spec Resin (Eichrom Technologies, LLC) as described in Argentino et al. (2021). The Sr was eluted with MilliQ® water. Through the chromatographic separation runs, n = 5 blanks were produced to monitor possible contamination during the procedure. Strontium isotope ratios ($^{87}Sr/^{86}Sr$) of 197 samples were measured with the Thermo Scientific NEPTUNE Plus multi-collector ICP-MS (MC-ICPMS) at the HUN-REN Institute for Nuclear Research (ATOMKI), Debrecen, Hungary. Isotopic ratios were corrected for instrumental mass discrimination using $^{88}Sr/^{86}Sr = 8.375209$ and by applying an interference correction for $^{87}Rb^+$, $^{84}Kr^+$ and $^{86}Kr^+$ with $^{85}Rb^+$ and $^{83}Kr^+$, respectively. The same method, shared between the two laboratories (Cavazzuti et al., 2021), was used to analyse n = 36 samples at the laboratory of the Centro Interdipartimentale Grandi Strumenti of Unimore using a Thermo Scientific NEPTUNE MC-ICPMS. Data reduction was performed with a modified version of the 'SrDR' spreadsheet (Lugli et al., 2020). Data are available at https://doi.org/10.5281/zenodo.17988601 (Scaggion et al., 2025a).

3.3 – Quality assessment of isotopic data

A poor chromatographic removal of Rb from sample could led to overestimate the $^{87}Sr/^{86}Sr$ ratio due to the isobaric interference of ^{87}Rb on ^{87}Sr. Before isotopic analyses, the Rb and Sr concentration of separate solutions were determined using a triple quadrupole ICPMS iCAP TQ (Thermo Fisher) at the laboratory of the Centro Interdipartimentale Grandi Strumenti of Unimore. The instrument was calibrated using a calibration curve for Rb, Sr and In from 1 to 1000 ppb, based on the international reference material IV-ICPMS-71A. Samples containing Rb higher than 0.5 ppb and with Rb/Sr ratio higher than 0.005 were reprocessed through a second chromatographic separation.

Possible contamination during the chromatographic separation has been evaluated with blank samples which were monitored using their signals V for ion counting during the isotopic analyses at the Centro Interdipartimentale Grandi Strumenti of Unimore. The signals of masses were indistinguishable from the instrument background.

To provide homogeneous reproducibility of the data, both laboratories share the same analytical protocol already used in other publications (e.g. Cavazzuti et al., 2021). The international Sr carbonate isotope Standard Reference Material NBS987 produced by the National Institute of Standard and Technology (NIST) was used as external standard for instrumental bias correction by both laboratories. Each session includes the analysis of three samples bracketed by the NBS-987 reference material. The instrumental bias was corrected independently in each analytical session normalizing to an accepted NBS-987 value of 0.710248 (McArthur et al., 2001). The average $^{87}Sr/^{86}Sr$ value of

https://doi.org/10.5194/essd-2026-136
Preprint. Discussion started: 4 March 2026

the NBS-987 of all the sessions in HUN-REN laboratory is 0.710329 ± 0.000006 and the average value of Unimore is 0.710250 ± 0.000014.

3.4 Statistical analysis and geospatial modelling

We built the Sr isoscapes of South America by combining the new Sr isotope dataset of 233 plant samples with literature data. The latter includes the Isoarch South America dataset (Salesse et al., 2018, 2020), excluding rock samples, and additional published sources (see Supplement Table S1) for a total of 1588 data points. The final dataset used for the model includes 1821 data from 883 sites (i.e. same coordinate samples) divided in 9 categories as follows: plant, fauna (archaeological remains, non-local excluded based on publication results), human (archaeological remains, non-local excluded), shell, snail, lichen, water and soil. The dataset is updated to September 2025. We constructed three different models, the first utilizing the whole dataset (hereafter 'All' dataset), the second limited to plant+fauna+lichen+human (661 sites) and the third using only the plant+lichen samples (531 sites). After a preliminary run of the random forest model, we noticed high prediction errors for $^{87}Sr/^{86}Sr$ values higher than 0.900. We thus excluded from the models n = 5 'anomalous' values of river waters from the Parguaza Batholith (Venezuela; $^{87}Sr/^{86}Sr > 0.900$) from Edmond et al. (1995). Here, we mainly focus on the plant+lichen isoscape, while the other models are reported in the Supplement Text S1. Note that the quantile colour scale is the same for each model, but rescaled to the values of the highlighted areas.

The dataset was regressed using the random forest machine-learning model from Bataille et al. (2020) in the R free software (version 4.0.5), which reconstructs the Sr isotopic ratio variability with a resolution of 1 km^2. The method uses external predictors variables to generate multiple decision trees using each time a random subset of data and covariates. For the models generation we used the global variables presented in Bataille et al. (2018, 2020) and Reich et al. (2024) as external predictors, filtering for each model the variables with high correlation (-0.80 > r > 0.80, Fig. 2) to avoid multicollinearity in the model and inflation of the variables importance (Strobl et al., 2008), as in Scaggion et al. (2025b). This resulted in the use of 14 external predictors, which were identical for the three models: *r.elevation*, *r.bulk*, *r.fert*, *r.dust*, *r.pet*, *r.cec*, *r.meanage_geol*, *r.ssaw*, *r.ph*, *r.srsrq1*, *r.clay*, *r.age*, *r.volc* and *r.GUM*.

We thus optimized the *mtyr* parameter for the random trees construction at 5 random variables at the time. The spatial-uncertaintly map was generated with the ranger package of Wright and Ziegler (2017), which calculates a quantile random forest regression, and then halving the random forest q0.84 - q0.16 difference (i.e., lower and upper limits of a ~68% interval: Funck et al., 2021 and Armaroli et al., 2024).

https://doi.org/10.5194/essd-2026-136
Preprint. Discussion started: 4 March 2026

The models were evaluated with a 10-fold cross validation by calculating the Root Mean Squared Error (RMSE). This method requires partitioning of the data into multiple subsets (folds) which are used as unknown to train and test the model, ensuring that it is not biased by single subsets. Using this approach, the model's accuracy and precision are tested across multiple subsets of data, providing a comprehensive assessment of the model's predictive capabilities.

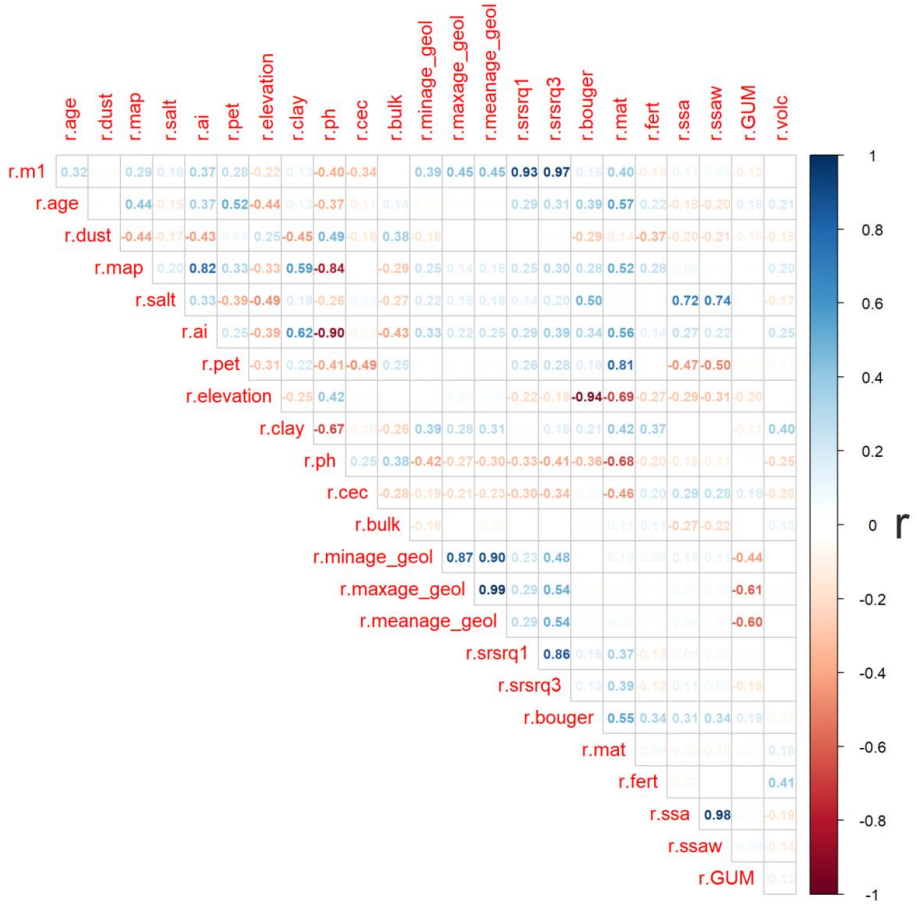

Figure 2: Pearson's correlation coefficients (r) of the external predictors used in the random forest model.

4 Results

4.1 $^{87}Sr/^{86}Sr$ of novel plant samples

Collected samples from the studied area yielded a broad range of $^{87}Sr/^{86}Sr$ ratios, between 0.70521 and 0.76039 with a median of 0.71360 (Fig. 3). The dataset shows an asymmetric distribution (kurtosis = 13.03, skewness = 2.77) with a long tail towards more radiogenic values (Fig. 3). A

https://doi.org/10.5194/essd-2026-136
Preprint. Discussion started: 4 March 2026

Open Access Earth System Science Data Discussions

Shapiro-Wilk test indicates significant deviation from normality (W = 0.733, $p < 0.01$). To facilitate interpretation, results of novel plant samples are presented here according to the underlying geological units or rock type as in Fig. 1 and Table 1. We stress however that plants were collected from soils developed on these units.

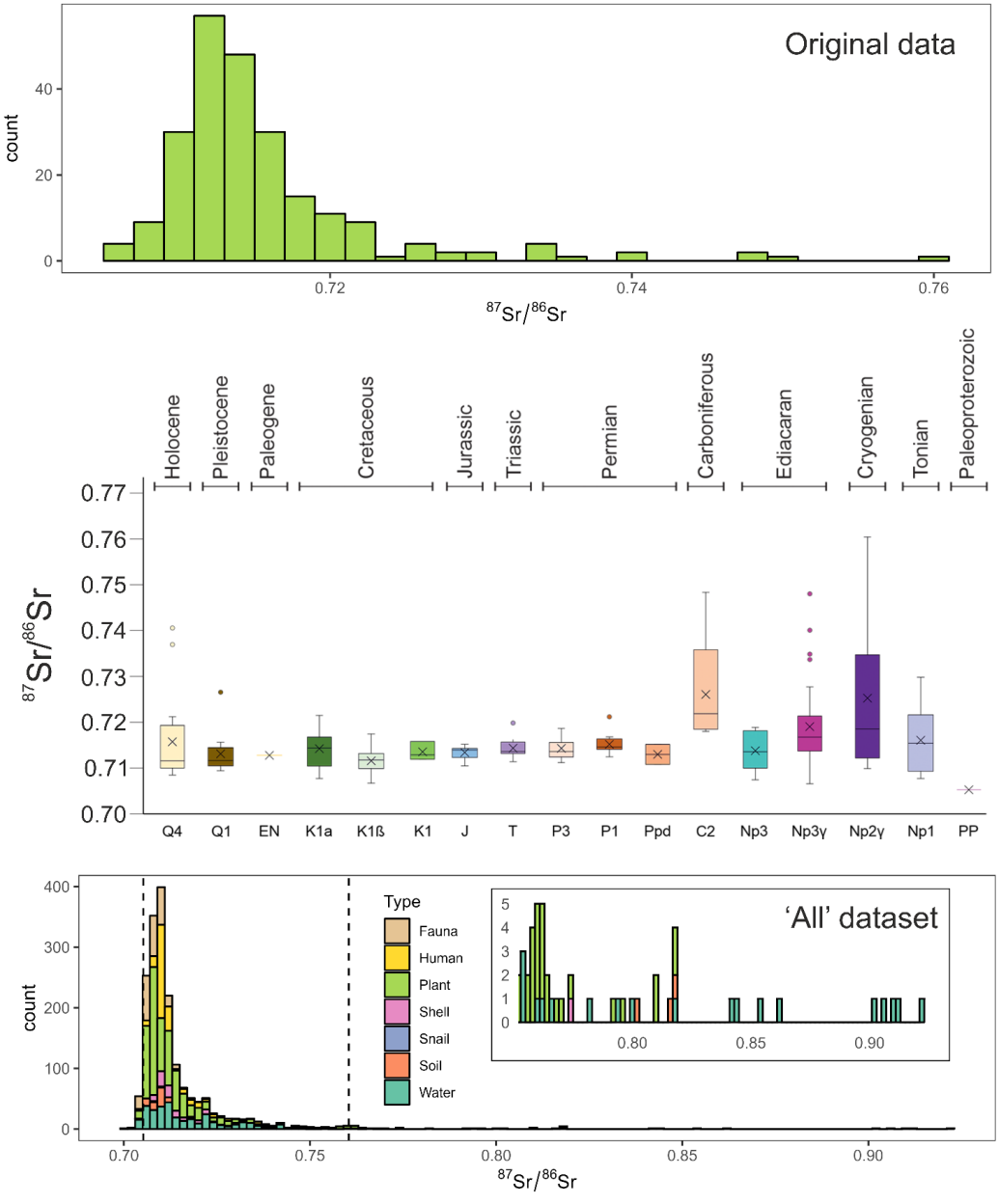

Figure 3: histogram of the whole dataset utilized to construct the isoscape model and of the new plant data. Boxplots of the plant samples from SC and RGS clustered by geological units as in Fig. 1: Q4-

https://doi.org/10.5194/essd-2026-136
Preprint. Discussion started: 4 March 2026

Holocene sediments; Q1-Pleistocene sediments; EN-Paleogene sedimentary; K1α-Serra Geral Formation, felsic; K1β-Serra Geral Formation, basic; K1-Cretaceous sedimentary; J-Jurassic sedimentary; T-Triassic sedimentary; P3-Late Permian sedimentary; P1-Early Permian sedimentary; Ppd-Permian andesite; C2-Carboniferous sedimentary; Np3-Ediacaran metasedimentary; Np3γ-Ediacaran metaigneous; Np2γ-Cryogenian metaigneous; Np1-Tonian metamorphic; PP-Paleoproterozoic basement.

Geological Unit	Sample Number	$^{87}Sr/^{86}Sr$ avg	st. dev.	Median	Lithology	Age
Q4	21	0.71569	0.00870	0.71155	Sediments	Holocene
Q1	11	0.71306	0.00481	0.71156	Sedimentary	Pleistocene
EN	1	0.71273	0.00002	0.71273	Sedimentary	Paleogene
K1α	15	0.71421	0.00412	0.71436	Magmatic - felsic	Cretaceous
K1β	46	0.71156	0.00226	0.71173	Magmatic - basic	Cretaceous
K1	3	0.71351	0.00202	0.71284	Sedimentary	Cretaceous
J	8	0.71335	0.00151	0.71387	Sedimentary	Jurassic
T	15	0.71432	0.00203	0.71359	Sedimentary	Triassic
Ppd	2	0.71336	0.00309	0.71336	Magmatic	Permian
P3	13	0.71429	0.00292	0.71358	Metasedimentary	Permian - Late
P1	14	0.71516	0.00204	0.71456	Metasedimentary	Permian - Early
C2	5	0.72604	0.01263	0.72181	Metasedimentary	Carboniferous
Np3γ	51	0.71892	0.00830	0.71659	Metaigneous	Ediacaran
NP3	8	0.71364	0.00428	0.71345	Metasedimentary	Ediacaran
NP2γ	10	0.72522	0.01727	0.71850	Metaigneous	Criogenian
Np1	9	0.71601	0.00732	0.71537	Metamorphic	Tonian
PP	1	0.70521	0.00002	0.70521	Metamorphic	Paleoproterozoic

Table 1: bioavailable Sr isotopic average composition of this work plant samples divided for the different geological super-units of the region as reported in Fig. 1. The order follows the stratigraphic order.

Plants from Holocene sediments (Q4) show values between 0.70843 and 0.74054, with an average of 0.71569 ± 0.00870 (n = 21; error calculated as standard deviation; Fig. 3; Table 1) while those from Pleistocene sediments (Q1, Q2, and Q3) have a narrower range from 0.70940 to 0.72650, with an average of 0.71306 ± 0.00481 (n=11), similar to only one Paleogene sample (EN) with a value of 0.71273 ± 0.00002 (Table 1). Plants from both sedimentary groups show anomalous values (Fig. 3).

https://doi.org/10.5194/essd-2026-136
Preprint. Discussion started: 4 March 2026

Samples from the Cretaceous felsic volcanics units of the Paraná LIP (K1α) show higher values (between 0.70766 and 0.72147; average of 0.71421 ± 0.00412, n =15) than those from the basic volcanics units (K1β; between 0.70666 and 0.71741; average of 0.71156 ± 0.00226, n =46; Fig. 3, Table 1). Plants from Cretaceous sediments of the Paraná Basin (K1) have similar K1α values, (0.71191 and 0.71578; average of 0.71351 ± 0.00202; n =3; Table 1), almost indistinguishable from those from Jurassic sediments (J; between 0.71045 and 0.71515; average of 0.71335 ± 0.00151; n = 8; Fig. 3, Table 1). Plants from other sedimentary units of the Paraná Basin (i.e., T, P1, and P3 units) show progressive radiogenic enrichment over time (averages at 0.71432 ± 0.00203; 0.71429 ± 0.00292; 0.71516 ± 0.00204, respectively). Samples from Permian volcanics (Ppd) have comparable values, between 0.71118 and 0.71554 with an average of 0.71336 ± 0.00309 (n=2; Table 1). In contrast, plants from Carboniferous sedimentary rocks (C2), have a distinct and more radiogenic signature between 0.71796 and 0.74832, average at 0.72604 ± 0.01263 (n = 5; Fig. 3, Table 1).

Samples collected from units of the Mantiqueira Province show broader ranges and generally higher values than those from Paraná Basin samples (except for C2 unit; Fig. 3). Plants from Ediacaran sediments of the Dom Feliciano Belt (Np3) yielded $^{87}Sr/^{86}Sr$ values between 0.70733 and 0.71871, with an average of 0.71364 ± 0.00428 (n = 8), while plants from metaigneous units (Np3γ) show higher and more variable values (0.7064 to 0.74790, with an average of 0.71892 ± 0.00830; n = 51; Fig. 3, Table 1). Samples from Cryogenian metaigneous units from the São Gabriel Terrane (Np2 γ) show the widest range in the dataset (from 0.70987 to 0.76039; average of 0.72522 ± 0.01727; n = 10; Fig. 3, Table 1). Plants from the Tonian metasedimentary units (Np1) show values between 0.70769 and 0.72978 with an average of 0.71601 ± 0.00732 (n = 9; Fig. 3, Table 1). Finally, the sample from the Paleoproterozoic basement (PP) yielded the lowest value of the entire dataset (0.70521 ± 0.00002; Table 1).

4.2 Random forest models

The three constructed isoscape models clearly distinguish the most radiogenic areas of the SC and RGS, which often correspond to the oldest geological units in the region (Fig.s 4 and 5). In all models, the associated errors are higher in these radiogenic areas (Fig.s 4 and 5), indicating lower predictive power of the models in these regions.

https://doi.org/10.5194/essd-2026-136
Preprint. Discussion started: 4 March 2026

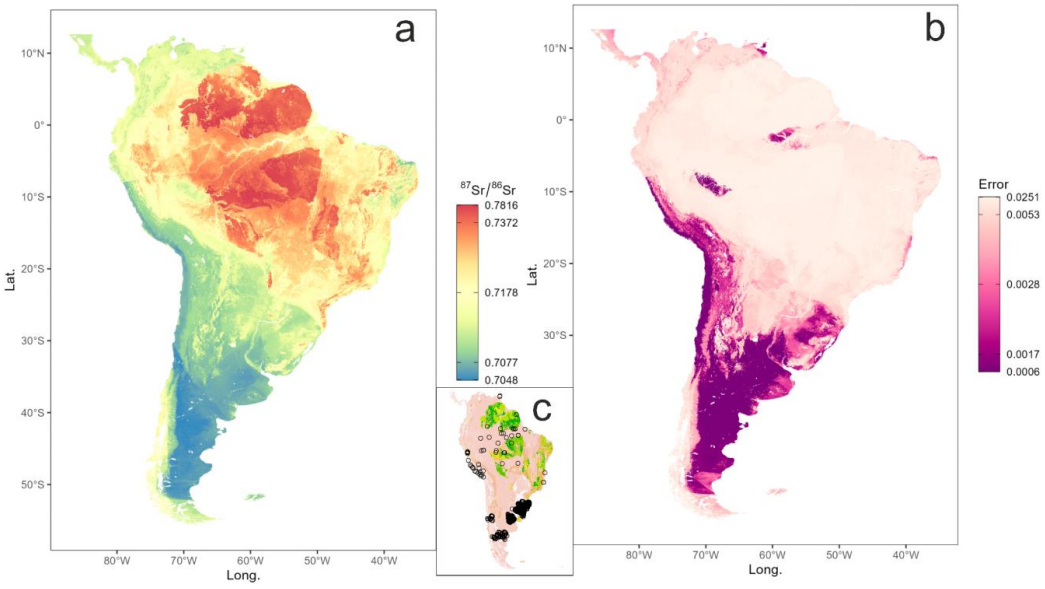

Figure 4: Spatial distribution of strontium isotopes in South America based on plant+lichen samples (n = 531 sites). Isoscape random forest model (a), associated spatial uncertainty map (b) and sample distribution (c).

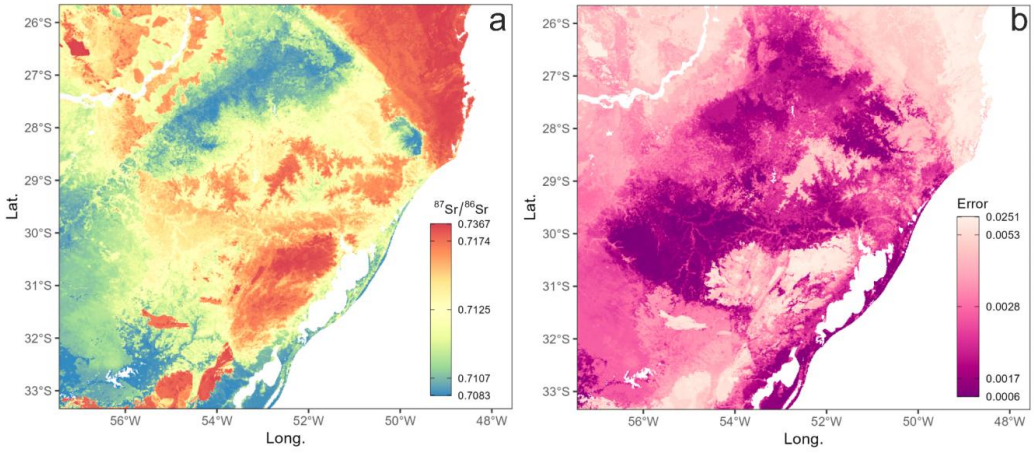

Figure 5: Spatial distribution of strontium isotopes in Santa Catarina and Rio Grande do Sul states based on plant+lichen samples (n = 531 sites). Isoscape random forest model (a) and associated spatial uncertainty map (b).

https://doi.org/10.5194/essd-2026-136
Preprint. Discussion started: 4 March 2026

Evaluation metrics reported in Table 2 show significant differences between the datasets: the model based on the 'All' dataset exhibits the lowest predictive power, with a RMSE of 0.0086 and an R^2 of 0.639, while the models built on the plant+fauna+lichen+human and the plant+lichen datasets show similar RMSE values of 0.0049 and 0.0054 respectively, and an R^2 of c.a. 0.76 each. The lower variance observed in these latter models likely reflects the smaller number and lower variability of samples compared to the 'All' dataset, which includes outliers with $^{87}Sr/^{86}Sr$ higher than 0.818 in water samples (Fig. 3).

Model	n. of sites	n. of predictors	RMSE	R^2	MAE
'All' dataset	883	14	0.0086	0.639	0.0037
Plants+Fauna+Human	661	14	0.0049	0.760	0.0023
Plants	531	14	0.0054	0.764	0.0027

Table 2: evaluation metrics of the models.

The evaluation of the predictive power of the independent variables using the Increase in Node Purity (IncNodePurity; Fig. 6; Supplement Text S1), shows that in the plant+fauna+lichen+human and plant+lichen models, the most relevant variables are *r.srsrq1* (predicted first quartile of the global $^{87}Sr/^{86}Sr$ bedrock model; Bataille et al., 2018) and *r.ph* (soil pH in H_2O solution x10; Bataille et al., 2020), both with IncNodePurity values just below 0.012 (Fig. 6), followed by *r.meanage_geol* (GLiM age attribute in Myrs; Bataille et al., 2020) and *r.cec* (cation exchange capacity; Bataille et al., 2020) with values of around 0.009, while all other variables have a contribution lower than 0.004 (Fig. 6). Notably, a 2D-Partial Dependence Plot (PDP, Fig. 7) shows a nonlinear interaction between *r.ph* and *r.srsrq1*, and indicates that the RF model predicts higher $^{87}Sr/^{86}Sr$ ratios when pH is low and - as expected - when the *r.srsrq1* bedrock model value is high. (Fig. 7).

https://doi.org/10.5194/essd-2026-136
Preprint. Discussion started: 4 March 2026

Open Access Earth System Science Data Discussions

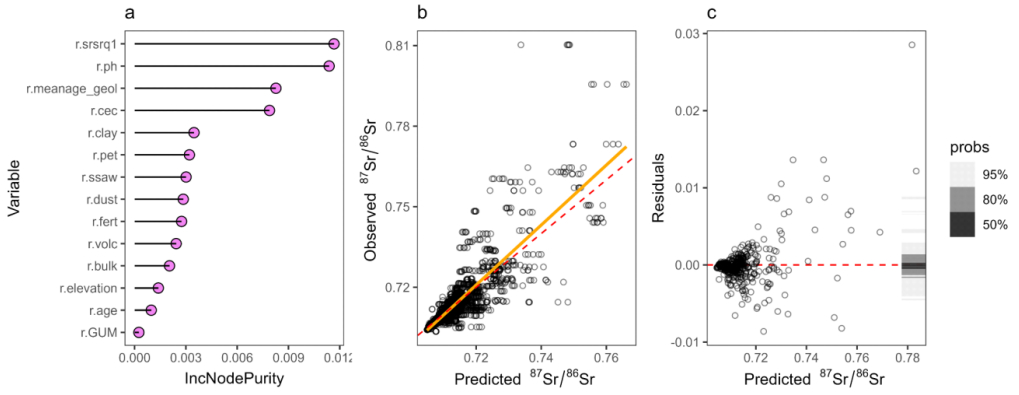

355

356 Figure 6: Predictive variables and model accuracy for random forest model based on plant+lichen
357 samples. Increase in Node Purity (IncNodePurity) of the n = 14 external predictors (a); cross-
358 validation scatterplot of observed vs. predicted $^{87}Sr/^{86}Sr$ values for the test–validation sample splits
359 (b); model residuals vs. predicted $^{87}Sr/^{86}Sr$ ratios (c).

360

361

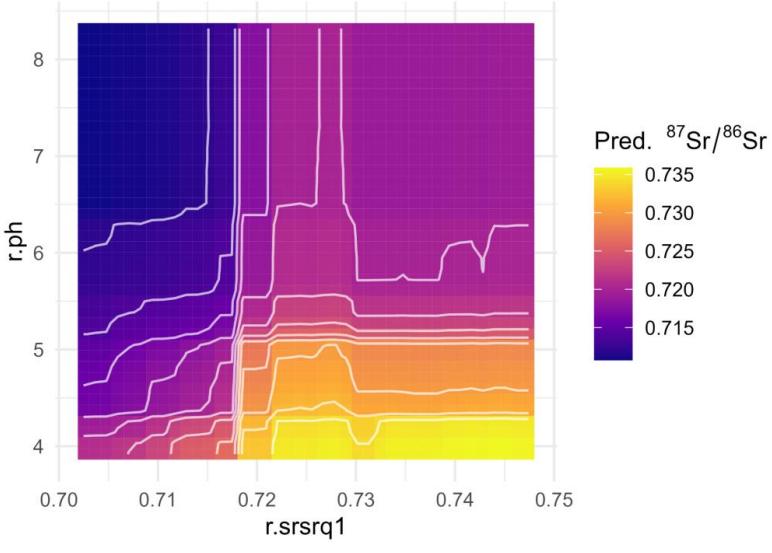

362

363 Figure 7: 2D Partial Dependence Plot for predictive variables *r.srsrq1* and *r.ph* for random forest
364 model based on plant+lichen samples.

365

366 In contrast, within the 'All' model the most predictive variable is *r.pet* (global potential evo-
367 transpiration; Bataille et al., 2018) with an IncNodePurity value equal to 0.038, followed by *r.ph* at

https://doi.org/10.5194/essd-2026-136
Preprint. Discussion started: 4 March 2026

0.020, *r.age* (Terrane age attribute in Myrs; Bataille et al., 2020) at 0.018, and *r.cec* and *r.srsrq1* at 0.015 (Supplement Text S1).

5 Discussion

5.1 Validation of the novel dataset against bedrock geology

Several inputs and processes govern the bioavailable Sr isotopic signature of local areas. However, considering a regional dataset, the bedrock geology is one of the main factors which govern the isotopic distribution (Vitousek et al., 1999; Voerkelius et al., 2010), and thus its relationship with the dataset could be a useful proxy to validate it.

The asymmetric statistical distribution of $^{87}Sr/^{86}Sr$ values observed in the novel dataset (Fig. 3), characterized by a long tail toward more radiogenic ratios, reflects the geological complexity of the area and the variety of contributing lithologies (Cryogenian igneous rocks, Ediacaran sedimentary sequences, Cretaceous volcanic flows, etc.). The presence of anomalous values among the plants growing on Holocene and Pleistocene sediments can be explained by the heterogeneity of the deposits (fluvial, marine, aeolian) and the characteristics of the parental lithologies.

The more radiogenic values of plants samples growth on soils from felsic igneous and metamorphic units compared to igneous basic and sedimentary units (e.g. units K1α, magmatic felsic, and K1β, magmatic basic with the same age), are consistent with well-known geological differentiation processes, as Rb commonly behaves as a more incompatible element in magmatic and metamorphic processes than Sr, thus becoming enriched during fractionation, forming rocks with higher or lower Rb content, which over time produce higher or lower $^{87}Sr/^{86}Sr$ ratios, as in K1α and K1β, respectively. Another aspect related to geology, is the increase of the $^{87}Sr/^{86}Sr$ ratio in rocks with time, which we expect to be reflected in the derived soil and then in the local vegetation. The plant dataset presented here follows this rule, with a general increase of the $^{87}Sr/^{86}Sr$ ratio as the bedrock is older in age (Fig. 3; Table 1) as observed for the Paranà Basin samples vs. Mantiqueira Province ones.

All these evidences suggest that the dataset is in overall agreement with bedrock geology which is the primary source of bioavailable Sr in nature.

5.2 Limits, advantages and predicting variables of the random forest models

Across the developed models, higher spatial uncertainties are associated with the most radiogenic areas of SC and RGS, generally corresponding to the oldest geological units in the area (Figs. 4, 5). This pattern, also reported in random forest models from the literature (e.g., Bataille et al., 2018; Gigante et al., 2023; Scaggion et al., 2025b), reflects the pronounced contrast in isotope composition between radiogenic bedrock and less radiogenic end-members such as aerosols, seawater, and

https://doi.org/10.5194/essd-2026-136
Preprint. Discussion started: 4 March 2026

precipitation. Such contrast complicates the mixing relationships processes that govern the bioavailable Sr isotope signature. Another parameter that influences model accuracy and associated errors is the uneven distribution of samples on a continental scale. Nonuniform sampling tends to introduce bias towards specific geological contexts, thereby limiting the ability to generalize predictions in unrepresented areas.

The improved performance observed in the plant+fauna+lichen+human and plant+lichen models, compared to the 'All' dataset, can be attributed to the reduced variability of the data, which limits the influence of outliers and improves the overall model stability. The absence of significant differences in the predictiveness between these two best performing models may reflect i) nonuniform and incomplete geographic coverage associated with water and soil sampling strategies, and ii) the limited representativeness of inorganic samples compared to biological and bioderived materials in representing the local terrestrial bioavailable Sr signature, as recently reported by Spies et al. (2025). In this regard, for random forest models, a smaller but more geologically representative dataset of biological samples is preferable over a larger but uneven dataset. Indeed, the latter reduces the representativeness of the isotopic variability and, consequently, compromises the accuracy and reliability of the models. Conversely, a smaller dataset anchored to the local geological context is more stable, robust, and useful for modelling (Marsh et al., 2025).

The predicted distribution map of the bioavailable $^{87}Sr/^{86}Sr$ isotope ratio shows a consistent correlation with the data obtained as a function of the variables *r.srsrq1* and *r.ph.* The combined marginal effect (Fig.7) between these two independent variables reveals that isotopic predictions are influenced by non-linear interactions between strontium isotope ratios (*r.srsrq1*) and soil pH (*r.ph*). Higher $^{87}Sr/^{86}Sr$ ratios correlate with more acidic soils, a pattern consistent with pedogenesis on ancient silicate igneous-metamorphic rocks. In the Amazon region, low pH values result from intense decomposition of organic matter, which leads to strong leaching of the bedrock and, consequently, increases Sr availability in the soil. The PDP (Fig. 7) explains how the geological context, pedogenic processes, and environmental conditions shape the spatio-temporal distribution of Sr isotope values.

Compared to existing Sr isoscapes, this study substantially improves both the spatial coverage and resolution of bioavailable predictions for South America, particularly southern Brazil. Although global or continental-scale isoscapes are essential for broader applications, developing regional models based on dense, geologically informed sampling offer much higher resolution and are essential for fine-scale provenance studies, such as intra-site archaeological mobility or ecological habitat use. Despite being focused on SC and the RGS regions, our dataset allowed us to obtain a reasonably robust continental-scale model with an R^2 of 0.764 (Fig.4). Our model compares positively with other continental-scale isoscapes (e.g. the bioavailable Sr isoscape of Australia, with

https://doi.org/10.5194/essd-2026-136
Preprint. Discussion started: 4 March 2026

an R^2 of 0.590; Dossetto et al., 2025). With this comparison, we do not intend to downplay the importance of large-scale modeling approaches, which are essential for global applications, but rather to highlight how carefully planned sampling strategies at the local level can provide robust, useful, and informative models at larger scales.

This highlights how carefully designed local sampling strategies not only strengthen regional provenance studies but also provide a reliable base for modeling at broader geographical scales.

6 Data availability

The bioavailable Sr plant isotope dataset of Santa Catarina and Rio Grande do Sul states analysed in this work and the raster files of the plant+lichen model are available at https://doi.org/10.5281/zenodo.17988601 (Scaggion et al., 2025a), The literature dataset is reported as Supplement Table S1.

7 Conclusion

This work presents a comprehensive dataset of 233 bioavailable $^{87}Sr/^{86}Sr$ values from plant samples collected across the main geological units of Santa Catarina and Rio Grande do Sul states (southern Brazil). The measured $^{87}Sr/^{86}Sr$ ratios in the terrestrial biosphere are consistent with lithological patterns, reflecting the pronounced geological heterogeneity of the region.

By integrating these new data with a multi-material dataset of literature data, we developed three isoscapes of bioavailable Sr distribution for South America and the studied region (c.a. 370,000 km^2) using advanced random forest modelling. Among the tested approaches, the plant+fauna+lichen+human and plant+lichen models achieved the best predictive performance, while the addition of water and soil reduced model performance due to their lower representativeness of locally bioavailable Sr.

Despite the limited dataset, the resulting models show robust predictive performance even at the continental scale. This result demonstrates how well-designed local sampling strategies can ensure reliable regional models that maintain their relevance and applicability at larger spatial scales. Beyond providing a new baseline for environmental, archaeological, and palaeoecological research in southern Brazil, our study highlights an important methodological insight: strategically constructed regional datasets can play a key role in refining continental-scale isoscapes. Future efforts should focus on expanding high resolution datasets across underrepresented geological domains.

Author Contribution

https://doi.org/10.5194/essd-2026-136
Preprint. Discussion started: 4 March 2026

C.S. was in charge of Conceptualization, Data curation, Formal analysis, Investigation, Methodology, Roles/Writing - original draft and Writing - review & editing;
T.G. was in charge of Conceptualization, Data curation, Formal analysis, Funding acquisition, Investigation, Methodology, Project administration, Resources, Supervision, Visualization, Roles/Writing - original draft and Writing - review & editing;
L.P. was in charge of Data curation, Formal analysis;
D.L. was in charge of Data curation;
M.C. was in charge of Data curation;
S.B. was in charge of Formal analysis;
S.B. was in charge of Data curation;
G.M. was in charge of Data curation;
M.C.P.S. was in charge of Data curation;
E.B. was in charge of Funding acquisition, Project administration;
A.C. was in charge of Formal analysis, Methodology, Supervision, Roles/Writing - original draft and Writing - review & editing;
F.L. was in charge of Conceptualization, Formal analysis, Data curation, Investigation, Methodology, Software, Visualization, Roles/Writing - original draft and Writing - review & editing;

Acknowledgement

CS, TG and EB were financially supported by European Union – Next Generation EU, Mission 4 Component 1 through grant PRIN2022 – HABITS 2022BC2Z5F project, CUP E53D23000130001 and CUP J53D23000140001. SBer is financed by the European Union - NextGenerationEU through the National Recovery and Resilience Plan (PNRR) - Mission 4, Component 2, Investment 1.3, titled: CHANGES - Cultural Heritage Active Innovation for Sustainable Society (PE0000020 - CUP J33C22002850006). AC received financial support from the European Union - Next-GenerationEU - National Recovery and Resilience Plan (NRRP) – MISSION 4 COMPONENT 2, INVESTIMENT N. 1.1, CALL PRIN 2022 PNRR D.D. 1409 14-09-2022 – “CAST Copper Accumulation, Supply, and Technology among Italian prehistoric societies", Codice progetto: P202275A2M, Decreto di finanziamento MUR D.D. n. 1388 del 1 settembre 2023 (CUP N. E53D23020120001).The funders had no role in study design, data collection and analysis, decision to publish, or preparation of the manuscript. SB and GM want to thank Antonino Vazzana and Owen Higgins.

References

https://doi.org/10.5194/essd-2026-136
Preprint. Discussion started: 4 March 2026

Argentino, C., Lugli, F., Cipriani, A., and Panieri, G.: Testing miniaturized extraction chromatography protocols for combined $^{87}Sr/^{86}Sr$ and $\delta^{88}/^{86}Sr$ analyses of pore water by MC-ICP-MS, Limnology and Oceanography: Methods, 19, 431-440, https://doi.org/10.1002/lom3.1043, 2021.

Armaroli, E., Lugli, F., Cipriani, A., and Tütken, T.: Spatial ecology of moose in Sweden: Combined Sr-O-C isotope analyses of bone and antler. PLoS One, 19(4):e0300867. https://doi.org/10.1371/journal.pone.0300867 PMID: 38598461, 2024.

Asrat ,S., Lucchini, F., Tafuri, M. A, Aureli, C., Gallinaro, M., Zerboni, A., Fusco, M., and Spinapolice, E. E: A strontium ($^{87}Sr/^{86}Sr$) isoscape of Southern Ethiopia: implications for hominin land use and faunal mobility patterns, Frontiers in Environmental Archaeology, 4, DOI=10.3389/fearc.2025.1499291, 2025.

Bataille, C. P., von Holstein, I. C. C., Laffoon, J. E., Willmes, M., Liu, X.-M., and Davies, G. R.: A bioavailable strontium isoscape for Western Europe: A machine learning approach, PLoS One, 13(5):e0197386. https://doi.org/10.1371/journal.pone.0197386 PMID: 29847595, 2018.

Bataille, C. P., Crowley, B. E., Wooller, M. J., and Bowen, G. J.: Advances in global bioavailable strontium isoscapes, Palaeogeography, Palaeoclimatology, Palaeoecology. 555:109849. https://doi.org/10.1016/j.palaeo.2020.109849, 2020.

Benson, S., Lennard, C., Maynard, P., and Roux, C.: Forensic applications of isotope ratio mass spectrometry--a review. Forensic Science International, 157(1), 1–22, https://doi.org/10.1016/j.forsciint.2005.03.012 PMID: 15919168, 2006.

Bentley, A. R.: Strontium Isotopes from the Earth to the Archaeological Skeleton: A Review. Journal of Archaeological Method and Theory, 13(3):135–87, https://doi.org/10.1007/s10816-006-9009-x, 2006.

Brito Neves, B. B., Fuck, R. A., and Pimentel, M. M.: The Brasiliano collage in South America: a review, Brazilian Journal of Geology, 44, 493-518, 2014.

https://doi.org/10.5194/essd-2026-136
Preprint. Discussion started: 4 March 2026

Bullen, T. D., Krabbenhoft, D. P., and Kendall, C.: Kinetic and mineralogic controls on the evolution of groundwater chemistry and $^{87}Sr/^{86}Sr$ in a sandy silicate aquifer, northern Wisconsin, USA, Geochimica et Cosmochimica Acta, 60(10), 1807–21, https://doi.org/10.1016/0016-7037(96)00052-x, 1996.

Capo, R. C., Stewart, B. W., and Chadwick, O. A.: Strontium isotopes as tracers of ecosystem processes: theory and methods. Geoderma, 82(1–3), 197–225, https://doi.org/10.1016/s0016-7061(97)00102-x, 1998.

Cavazzuti, C., Hajdu, T., Lugli, F., Sperduti, A., Vicze, M., Horváth A, Major, I., Molnár, M., Palcsu, L., and Kiss, V.: Human mobility in a Bronze Age Vatya 'urnfield' and the life history of a high-status woman, PLoS ONE, 16(7): e0254360, https://doi.org/10.1371/journal.pone.0254360, 2021.

Cerva-Alves, T., Hartmann, L. A., Lana, C., Queiroga, G. N., Maciel, L. A. C., Leandro, C. G., and Savian, J. F.: Rutile and zircon age and geochemistry in the evolution of the juvenile São Gabriel Terrane early in the Brasiliano Orogeny, Journal of South American Earth Sciences, 112(1), 103505 ISSN 0895-9811, https://doi.org/10.1016/j.jsames.2021.103505, 2021.

Crowley, B. E., Miller, J. H., and Bataille, C. P.: Strontium isotopes ($^{87}Sr/^{86}Sr$) in terrestrial ecological and palaeoecological research: empirical efforts and recent advances in continental-scale models. Biological Reviews, 92(1), 43–59, https://doi.org/10.1111/brv.12217 PMID: 26392144, 2017.

Dickin, A. P.: Radiogenic Isotope Geology. third edition. McMaster University, editor. Cambridge: Cambridge University Press; 2018.

Dosseto, A., Dux, F., Bataille, C., and de Caritat, P.: A bioavailable strontium isoscape of Australia, Earth System Science Data, 17, 4865–4880, https://doi.org/10.5194/essd-17-4865-2025, 2025.

Edmond, J. M., Palmer, M. R., Measures, C. I., Grant, B., and Stallard, R. F.: The fluvial geochemistry and denudation rate of the Guayana Shield in Venezuela, Colombia, and Brazil, Geochimica et Cosmochimica Acta, 59, 16, 3301-3325. 10.1016/0016-7037(95)00128-m, 1995.

https://doi.org/10.5194/essd-2026-136
Preprint. Discussion started: 4 March 2026

568 Faure, G., and Mensing, T. M.: Isotopes: Principles and Applications. third edition. editor. New York:
569 John Wiley & Sons INC; 2005.
570
571 Fietzke, J., and Eisenhauer, A.: Determination of temperature-dependent stable strontium isotope
572 ($^{88}Sr/^{86}Sr$) fractionation via bracketing standard MC-ICP-MS, Geochemistry Geophysics
573 Geosystems, 7(8), https://doi.org/10.1029/2006gc001243, 2006.
574
575 Frei, K. M., and Frei, R.: The geographic distribution of strontium isotopes in Danish surface waters
576 – A base for provenance studies in archaeology, hydrology and agriculture, Applied Geochemistry,
577 26(3), 326–40, https://doi.org/10.1016/j.apgeochem.2010.12.006, 2011.
578
579 Gigante, M., Mazzariol, A., Bonetto, J., Armaroli, E., Cipriani, A., and Lugli, F.: Machine learning-
580 based Sr isoscape of southern Sardinia: A tool for bio-geographic studies at the Phoenician-Punic site
581 of Nora. PLoS One, 18(7):e0287787, https://doi.org/10.1371/journal.pone.0287787 PMID:
582 37467179, 2023.
583
584 Giovanardi, T., da Costa, P. C. C., Girardi, V. A. V., Weska, R. K., Vasconcelos, P. M., Thiede, D.
585 S., Mazzucchelli, M., and Cipriani, A.: Age, geochemistry and mantle source of the Alto Diamantino
586 basalts: Insights on NW Paraná Magmatic Province, Lithos, 426-427, 106797, 2022
587
588 Gomes, A. S., and Vasconcelos, P. M.: Geochronology of the Paraná-Etendeka large igneous
589 province, Earth Sciences Review, 220, 103716 https://doi.org/10.1016/j.earscirev.2021.103716,
590 2021.
591
592 Heilbron, M., Pedrosa-Soares, A. C., Campos Neto, M. C., Silva, L. C., Trouw, R. A. J., and Janasi,
593 V. A.: Província Mantiqueira. In: Mantesso-Neto V., Bartorelli A., Carneiro C.D.R., Brito Neves B.B.
594 (eds.) Geologia do Continente Sul-Americano: Evolução da Obra de Fernando Flávio Marques de
595 Almeida, São Paulo, Beca, 203-234, 2004.
596
597 Hobson, K. A.: Tracing origins and migration of wildlife using stable isotopes: a review, Oecologia,
598 120(3), 314–26, https://doi.org/10.1007/s004420050865 PMID: 28308009, 1999.
599
600 Holz, M., França, A. B., Souza, P. A., Iannuzzi, R., and Rohn, R: A stratigraphic chart of the Late
601 Carboniferous/Permian succession of the eastern border of the Paraná Basin, Brazil, South America,

https://doi.org/10.5194/essd-2026-136
Preprint. Discussion started: 4 March 2026

602 Journal of South American Earth Sciences, 29(2), 381-399, ISSN 0895-9811,
603 https://doi.org/10.1016/j.jsames.2009.04.004, 2010.
604
605 Hoogewerff, J. A., Reimann, C., Ueckermann, H., Frei, R., Frei, K. M., van Aswegen, T., Stirling,
606 C., Reid, M., Clayton, A., and Ladenberger, A.: Bioavailable $^{87}Sr/^{86}Sr$ in European soils: A baseline
607 for provenancing studies, Science of The Total Environment, 672, 1033–44,
608 https://doi.org/10.1016/j.scitotenv.2019.03.387 PMID: 30999220, 2019.
609
610 Hughes, J. M., and Rakovan, J.: The Crystal Structure of Apatite, Ca5(PO4)3(F,OH,Cl), Reviews in
611 Mineralogy and Geochemistry, 48(1), 1–12. https://doi.org/10.2138/rmg.2002.48.1, 2002.
612
613 Lahtinen, M., Arppe, L., and Nowell, G.: Source of strontium in archaeological mobility studies—
614 marine diet contribution to the isotopic composition, Archaeological and Anthropological Sciences,
615 13(1). https://doi.org/10.1007/s12520-020-01240-w, 2020.
616
617 Loponte, D., Carbonera, M., and Radaeski, J.: The Guaraní expansion in the Upper Uruguay River.
618 Chronology, colonization strategies, social impacts and environmental changes, Journal of
619 Archaeological Science: Reports, 60:104826. https://doi.org/10.1016/j.jasrep.2024.104826, 2024.
620
621 Luchetti, A. C. F., Nardy, A. J. R., and Madeira, J.: Silicic, high- to extremely high-grade ignimbrites
622 and associated deposits from the Paraná Magmatic Province, southern Brazil, Journal of Volcanology
623 and Geothermal Research, 355, 270–286, 2018.
624
625 Lugli, F., Weber, M., Giovanardi, T., Arrighi, S., Bortolini, E., Figus, C., Marciani, G., Oxilia, G.,
626 Romandini, M., Silvestrini, S., Jochum, K. P., Benazzi, S., and Cipriani, A.: Fast offline data
627 reduction of laser ablation MC-ICP-MS Sr isotope measurements: Via an interactive Excel-based
628 spreadsheet 'SrDR', Journal Of Analytical Atomic Spectrometry, 35:5, 852-862,
629 https://doi.org/10.1039/C9JA00424F, 2020.
630
631 Lugli, F., Cipriani, A., Bruno, L., Ronchetti, F., Cavazzuti, C., and Benazzi, S.: A strontium isoscape
632 of Italy for provenance studies, Chemical Geology, 587:120624.
633 https://doi.org/10.1016/j.chemgeo.2021.120624, 2022.
634

https://doi.org/10.5194/essd-2026-136
Preprint. Discussion started: 4 March 2026

635 Makarewicz, C. A., and Sealy, J.: Dietary reconstruction, mobility, and the analysis of ancient skeletal
636 tissues: Expanding the prospects of stable isotope research in archaeology, Journal of Archaeological
637 Science, 56, 146–58, https://doi.org/10.1016/j.jas.2015.02.035, 2015.
638
639 Marsh, E. J., Cardillo, M., Knudson, K. J., Dahlstedt, A., and Barberena, R.: A bioavailable strontium
640 isoscape for the Andes based on machine learning, Journal of Archaeological Science, 184, 106410,
641 ISSN 0305-4403, https://doi.org/10.1016/j.jas.2025.106410, 2025.
642
643 McArthur, J. M., Howarth, R. J., and Bailey, T. R.: Strontium isotope stratigraphy: LOWESS version
644 3: best fit to the marine Sr-isotope curve for 0–509 Ma and accompanying look-up table for deriving
645 numerical age, The Journal of Geology, 109(2), 155-170, 2001.
646
647 Medeiros, V. C., Santos, F. G., Quadros, M. L. E. S., Espirito Santo, E. B. S., Silva, M. A., Moreira.
648 G., Santana, J. S., Domingos, N. R. R., Barros, T. S. C., Santos, P. A., Almeida, M. E., and Wanderley,
649 A. A.: Mapa Geológico do Brasil. Escala 1:5.000.000. Salvador: SGB-CPRM, 2025.
650
651 Milani, E.J., Melo, J.H.G., de Souza, P.A., de Fernandes, L.A., and França, A.B.: Bacia do Paraná.
652 Boletim de Geociências da Petrobras, 15(2), 265-287, 2007.
653
654 Peate, D.W., Hawkesworth, C.J., and Mantovani, M.S.M.: Chemical stratigraphy of the Paraná lavas
655 (South America): classification of magma types and their spatial distribution. Bulletin of
656 Volcanology, 55, 119–139, 1992.
657
658 Philipp, R. P., Pimentel, M. M., and Basei, M. A. S.: The Tectonic Evolution of the São Gabriel
659 Terrane, Dom Feliciano Belt, Southern Brazil: The Closure of the Charrua Ocean, S. Siegesmund
660 (Ed.), Geology of Southwest Gondwana, Regional Geology Reviews, 243-265, 2018.
661
662 Piccirillo, E.M., and Melfi, A.J.: The Mesozoic Flood Volcanism of the Paraná Basin: Petrogenetic
663 and Geophysical Aspects. Universidade de São Paulo, São Paulo, p. 600, 1988.
664
665 Pors Nielsen, S.: The biological role of strontium, Bone, 35(3), 583–8.
666 https://doi.org/10.1016/j.bone.2004.04.026 PMID: 15336592, 2004.
667

https://doi.org/10.5194/essd-2026-136
Preprint. Discussion started: 4 March 2026

668 Poszwa, A., Dambrine, E., Pollier, B., and Atteia, O.: A comparison between Ca and Sr cycling in
669 forest ecosystems, Plant and Soi, 225, 299–310, https://doi.org/10.1023/a:1026570812307, 2000.
670
671 Reich, M.S., Ghouri, S., Zabudsky, S., Hu, L., Le Corre, M., Ng'iru I, Benyamini, D., Shipilina, D.,
672 Collins, S. C., Martins, D. J., Vila, R., Talavera, G., and Bataille, C. P.: Trans-Saharan migratory
673 patterns in Vanessa cardui and evidence for a southward leapfrog migration, iScience, 27(12),
674 111342, https://doi.org/10.1016/j.isci.2024.111342 PMID: 39654635, 2024.
675
676
677 Salesse, K., Fernandes, R., de Rochefort, X., Brůžek, J., Castex, D., and Dufour, É.: isoarch.org: An
678 open-access and collaborative isotope database for bioarcheological samples from Graeco-Roman
679 World and its margins, Journal of Archaeological Science: Reports, 19, 1050-1055, 2018.
680
681 Salesse, K., Fernandes, R., de Rochefort, X., Brůžek, J., Castex, D., and Dufour, É.: isoarch.org
682 (v.1.1), accessed 10/15/2025, 2020.
683
684 Scaggion, C., Giovanardi, T., Palcsu, L., Cipriani, A., and Lugli, F.: Bioavailable Sr isotopes of plants
685 from Rio Grande do Sul and Santa Catarina states (Brazil, South America) and related isoscape raster
686 files (Version 01) [Data set]. Zenodo, 2025a. https://doi.org/10.5281/zenodo.17988601
687
688 Scaggion, C., Giovanardi, T., Loponte, D., Carbonera, M., Armaroli, E., Bernardini, S., Benazzi, S.,
689 Gascue, A., Acosta, A., Marciani, G., Bortolini, E., Cipriani, A., and Lugli, F.: Random forest-based
690 bioavailable strontium isoscape for environmental and archaeological applications in central eastern
691 Argentina and western Uruguay, Plos One, 20(7), e0326047,
692 https://doi.org/10.1371/journal.pone.0326047, 2025b.
693
694 Scherer, C. M S., Reis, A. D., Horn, B. L. D., Bertolini, G., Lavina, E. L. C., Kifumbi, C., and Aguilar,
695 C. G.: The stratigraphic puzzle of the permo-mesozoic southwestern Gondwana: The Paraná Basin
696 record in geotectonic and palaeoclimatic context, Earth-Science Reviews, Volume 240, 104397,
697 ISSN 0012-8252, https://doi.org/10.1016/j.earscirev.2023.104397, 2023.
698
699 Schwarcz, H. P., White, C. D., and Longstaffe, F. J.: Stable and Radiogenic Isotopes in Biological
700 Archaeology: Some Applications. Isoscapes. Dordrecht: Springer Netherlands; p. 335–356.
701 https://doi.org/10.1007/978-90-481-3354-3_16, 2010.

https://doi.org/10.5194/essd-2026-136
Preprint. Discussion started: 4 March 2026

Spies, M. J., Alblas, A., Ambrose, S. H., Barakat, S., Barberena, R., Bataille, C. P., Bowen, G. J., Britton, K., Cawthra, H., Diamond, R., Dosseto, A., Evans, J. A., Fisher, E., Gray, K., Heddell-Stevens, P., Holt, E., James, H. F., Janzen, A., Le Corré, M., le Roux, P., Lee-Thorp, J., Mackay, A., McNeill, P. J., Montgomery, J., Mugabe, B., Oelze, V. M., Pfab, M., Richards, M. P., Samec, C. T., Santana-Sagredo, F., Serna, A., Stantis, C., Snoeck, C., Stewart, B., Stuurman, C., Tarrant, D., West, A. G., Winter-Schuh, C., and Sealy, J.: Strontium isoscapes for provenance, mobility and migration: the way forward, Royal Society Open Science, 12(6), 12250283 http://doi.org/10.1098/rsos.250283, 2025.

Strobl, C., Boulesteix, A.-L., Kneib, T., Augustin, T., and Zeileis, A.: Conditional variable importance for random forests, BMC Bioinformatics, 9, 307, https://doi.org/10.1186/1471-2105-9-307 PMID: 18620558, 2008.

Vitousek, P. M., Kennedy, M. J., Derry, L. A., and Chadwick, O. A.: Weathering versus atmospheric sources of strontium in ecosystems on young volcanic soils, Oecologia, 121(2), 255–9. https://doi.org/10.1007/s004420050927 PMID: 28308565, 1999.

Voerkelius, S., Lorenz, G. D., Rummel, S., Quétel, C. R., Heiss, G., Baxter, M., Brach-Papa, C., Deters-Itzelsberger, P., Hoelzl, S., Hoogewerff, J., Ponzevera, E., Van Bocxstaele, M., and Ueckermann, H.: Strontium isotopic signatures of natural mineral waters, the reference to a simple geological map and its potential for authentication of food, Food Chemistry, 118(4), 933–40, https://doi.org/10.1016/j.foodchem.2009.04.125, 2010.

Weiner, S., and Wagner, H. D.: THE MATERIAL BONE: Structure-Mechanical Function Relations, Annual Review of Materials Research, 28(1), 271–98, https://doi.org/10.1146/annurev.matsci.28.1.271, 1998.

Wildner, W., Camozzato, E., Toniolo, J. A., Binotto, R. B., Iglesias, C. M. F., and Laux, J. H.: Mapa geologoco do estado de Santa Catarina. Porto Alegre: CPRM. Escala 1:500000. Programa geologia do Brasil. Subprograma de Cartografia Geologica Regional, 2014.

https://doi.org/10.5194/essd-2026-136
Preprint. Discussion started: 4 March 2026

734 Wildner, W., Ramgrab, G. E., Lopes, R. C., Iglesias, C. M. F., and Laux, J. H.: Mapa geológico do
735 estado de Rio Grande do Sul. Porto Alegre: CPRM. Escala 1:750000. Programa geologia do Brasil.
736 Subprograma de Cartografia Geologica Regional, 2013.
737
738 White, P. J., and Broadley, M. R.: Calcium in plants, Annals of Botany, 92(4), 487–511,
739 https://doi.org/10.1093/aob/mcg164 PMID: 12933363, 2003.
740
741 Wright, M. N., and Ziegler, A.: ranger: A Fast Implementation of Random Forests for High
742 Dimensional Data in C++ and R, Journal of Statistical Software, 77(1), 1-17,
743 https://doi.org/10.18637/jss.v077.i01, 2017.
744

745 **Supplement**

746 Supplement Table S1: literature dataset of $^{87}Sr/^{86}Sr$ from South America used to construct the random
747 forest models. The dataset is updated in September 2025.
748
749 Supplement Text S1: models and parameters for the ‘All’ and plant+fauna+lichen+human dataset.